

# Emergences of C IV narrow absorption troughs in the quasar SDSS J095254.10+021932.8

Zhi-Fu Chen<sup>1,2\*</sup>, Mu-Sheng Li<sup>2</sup>, Wei-Rong Huang<sup>2</sup>, Cai-Juan Pan<sup>1</sup>, You-Bing Li<sup>3</sup>

<sup>1</sup> *Department of Physics and Telecommunication Engineering, Baise University, Baise, 533000, China*

<sup>2</sup> *Center for Astrophysics, Guangzhou University, Guangzhou 510006, China*

<sup>3</sup> *City Construction College of Guangzhou, Guangdong, 510925, China*

4 June 2021

## ABSTRACT

In this paper, we report on two C IV narrow absorption systems emerging from the spectrum of the quasar SDSS J095254.10 +021932.8, which are located at  $z_{\text{abs}} = 2.0053$  and  $z_{\text{abs}} = 1.8011$ , respectively. These features have velocity offsets of  $\sim 13,800$  and  $\sim 34,700 \text{ km s}^{-1}$  with respect to the quasar, and show obviously partial coverage to the background emission sources. The two C IV absorption systems are imprinted on the spectrum obtained by the Sloan Digital Sky Survey (SDSS) III on 2011 March 25, which cannot be observed from the spectrum obtained by SDSS-I/II on 2000 December 30. The time interval of the two SDSS observations is 1186.4 d at the quasar rest frame. Because the continuum radiation, broad emission lines and mass accretion rate are stable for the two observations, together with the time interval of observations, we believe that the observed spectral variations are less likely to be caused by the changes in the ionization states of the absorbing gas or by a new outflow, arising from the situation where there was previously no outflow at all. Instead, they probably arise from the motions of multiple streaming gas across the sightline of the quasar.

**Key words:** galaxies: active — quasars: absorption lines — quasars: individual (J095254.10+021932.8)

## 1 INTRODUCTION

Active galaxies are powered by accreting material on to the corresponding central supermassive black holes. The gas not only falls into the black hole, but can also be lifted off the accretion disc under some mechanisms in powerful winds/outflows. Outflows seem to be the fundamental component of quasar systems, and are present in at least 50 per cent of optically selected quasars (Crenshaw, Kraemer & George 2003; Ganguly & Brotherton 2008; Nestor, Hamann & Rodríguez Hidalgo 2008). It is widely accepted that the outflows play an important role in regulating the growth of supermassive black holes by carrying away the angular momentum (Silk & Rees 1998; King 2003). Moreover, the outflows might inject enough kinetic energy and metal-rich gas into the host galaxies, influencing the star formation, the enrichment of the surrounding intergalactic medium, and so on (e.g. Di Matteo, Springel & Hernquist 2005; Bower et al. 2006; Moll et al. 2007; Dunn et al. 2012). Therefore, it

is important to understand the properties and evolution of quasar outflows.

Unfortunately, the nature and origin of quasar outflows are still mysterious. Some models suggest that the quasar outflows are physically related to the gas lifted off the accretion disc, which would be driven by the radiation pressure, magnetic forces, or a combination of these (Arav, Li & Begelman 1994; de Kool & Begelman 1995; Murray et al. 1995; Murray & Chiang 1997; Proga, Stone & Kallman 2000; Everett 2005). Here, the radiation pressure seems to play a dominant role (Laor & Brandt 2002; Hamann et al. 2011). The quasar outflows are detected most conspicuously via blueshifted metal absorption lines. These absorption lines imprint on the quasar spectra in different forms based on linewidths: broad absorption lines (BALs) with absorption troughs that are broader than  $2000 \text{ km s}^{-1}$  at depths  $> 10$  per cent below the continuum; narrow absorption lines (NALs) with velocity widths of a few hundred  $\text{km s}^{-1}$ ; intermediate width absorption lines (mini-BALs; e.g. Weymann et al. 1991; Jannuzi et al. 1996; Yuan et al. 2002; Wise et al. 2004; Misawa et al. 2008; Hamann et al. 2011). It is possible that the different types of lines arise in

\* E-mail:zhichenfu@126.com

the same quasar outflow but are viewed at different angles (Murray et al. 1995). Alternatively, they might be formed in the same quasar outflow but at different evolutionary stages, where NALs and mini-BALs appear near the beginning or end stages of a more powerful BAL outflow (e.g. Hamann & Sabra 2004; Hamann et al. 2008).

BALs are undoubtedly intrinsic to quasars. Therefore, many previous studies of outflow absorption lines have focused on BALs (e.g. Gibson et al. 2008; Moe et al. 2009; Capellupo et al. 2011, 2012, 2013). However, it is difficult to distinguish intrinsic NALs from cosmologically intervening NALs, which are often believed to be associated with cosmologically intervening galaxies. In spite of this difficulty, many works on quasar outflows have been carried out using NALs (e.g. Narayanan et al. 2004; Misawa et al. 2007; Hamann et al. 2011; Chen, Qin & Gu 2013). These intrinsic absorption lines, which are highly ionized (e.g. O VIII, Fe XVII), are mainly detected in the high-energy band spectra (e.g. X-ray spectra), while the transitions by ions with low ionization potential (e.g. C IV, S IV, N V, O VI) can be observed in both the X-ray and ultraviolet (UV) spectra. The absorption lines, which are imprinted in both the UV and X-ray spectra with similar velocities relative to the quasars, imply an underlying relationship between the narrow absorption lines in the UV and X-ray spectra (Mathur et al. 1994; Mathur, Elvis & Wilkes 1995; Sabra et al. 2003; Tombesi et al. 2011a,b; Gupta et al. 2013a).

Line variability is likely to be a good method for investigating quasar outflows, because it can constrain the outflow dynamics, stability, location and basic physical properties. The variability of absorption lines imprinted on the quasar spectra could be related to the fluctuation of the background emission sources. This would induce a variation in the ionization states of the absorbing gas and/or the proper motion of absorbers, which could give rise to changes in the column density or changes in covering factors.

Time variations of BALs and NALs are relatively common, but the extreme changes in the absorption profiles in the near-UV and optical spectra are rare. We are aware that only a few cases of the disappearance (e.g. Junkkarinen et al. 2001; Lundgren et al. 2007; Hall et al. 2011; Filiz Ak et al. 2012) and emergence (Ma 2002; Hamann et al. 2008; Leighly et al. 2009; Krongold, Binette & Hernandez-Ibarra 2010; Rodríguez Hidalgo, Hamann & Hall 2011; Vivek et al. 2012) of BALs have been reported in the near-UV and optical spectra. These can be detected on time-scales of years at the quasar rest frame.

It would be very interesting to detect the emergence of absorption lines because the variability programmes usually monitor quasars for which the absorption lines have already been detected. In this paper, we report on two emergence events of CIV absorption systems, which are imprinted on the spectrum of the quasar SDSS J095254.10 +021932.8. In Section 2, we provide a spectral analysis, and we present a discussions and conclusions in Sections 3 and 4, respectively. Throughout this paper, we adopt the cosmological parameters  $\Omega_{\Lambda} = 0.7$ ,  $\Omega_M = 0.3$ , and  $h = 0.7$ .

## 2 SPECTRAL ANALYSIS

The Baryon Oscillation Spectroscopic Survey (BOSS), which is part of the Sloan Digital Sky Survey (SDSS) III (Eisenstein et al. 2011), aims to obtain the spectra of over 150 000 quasars  $z > 2.2$  (Ross et al. 2012). The SDSS Data Release 9 is the first release of BOSS spectroscopy to the public, which contains  $\sim 87,000$  quasars detected over  $3,275 \text{ deg}^2$  (Pâris et al. 2012). The 7932 quasars obtained by SDSS-I/II (York et al. 2000; Abazajian et al. 2009; Schneider et al. 2010) have been reobserved during the two first years of BOSS.

Quasar spectra with a higher signal-to-noise ratio (S/N) are useful for the detection of weak absorption lines. We aim to detect C IV  $\lambda\lambda 1548, 1551$  absorption doublets on quasar spectra with high S/N and with two observations. Specifically, we select quasars from the SDSS quasar catalogue, which have been observed by both SDSS-I/II and SDSS-III, and whose median S/N over the whole spectrum is greater than 15 (the median S/N over the whole spectrum is defined by Pâris et al. 2012). Because of the significant systematic sky-subtraction residual longward of 7000 Å and the noise region shortward of 4000 Å in many SDSS-I/II spectra, we constrain the wavelength range detected C IV  $\lambda\lambda 1548, 1551$  absorption doublets from 4,000 Å to 7,000 Å at observed frame. The O I  $\lambda 1302$  and Si II  $\lambda 1304$  pair has a wavelength separation similar enough to that of the C IV  $\lambda\lambda 1548, 1551$ . In order to avoid the Ly $\alpha$  forest, O I  $\lambda 1302$  and Si II  $\lambda 1304$  absorption lines, we exclude the spectral region shortward of 1350 Å at rest-frame. Based on above selection criteria, there are 680 appropriate quasars to search for C IV  $\lambda\lambda 1548, 1551$  absorption doublets.

Following some previous works (e.g. Nestor, Turnshek & Rao 2005; Quider et al. 2011; Chen et al. 2013), we invoke the cubic splines (for the underlying continuum, see Willian et al. 1992 for details) plus the Gaussians (for the emission and broad absorption figures) to fit a pseudo-continuum for each of the 680 quasar spectra. This is used to normalize the spectral fluxes and flux uncertainties. The process is iterated several times to improve the fits of both the cubic splines and the Gaussians. We detect absorption figures on the pseudo-continuum normalized spectra. During the detecting, we first mask out the three times flux uncertainty levels ( $3\sigma$ ), which have been normalized by the pseudo-continua, and we rule out the absorption figures located within  $3\sigma$ . In the second step, we flag the absorption figures imprinted on the SDSS-III spectra but not on those of SDSS-I/II, and we rule out absorption figures with absorption troughs that are broader than  $1000 \text{ km s}^{-1}$  at depths  $> 10\%$  below the continuum. In the third step, we invoke a Gaussian component to fit each absorption trough, and we rule out the trough with  $FWHM > 600 \text{ km s}^{-1}$ . Then, in the fourth step, we search for the C IV  $\lambda\lambda 1548, 1551$ . We find only one doublet, which was imprinted on the quasar spectrum of J095254.10 +021932.8. This C IV  $\lambda\lambda 1548, 1551$  absorption doublet (the *R* - component shown in Fig. 2) is located at  $z_{\text{abs}} = 2.0053$  and has  $FWHM_{\lambda 1548} = 420 \text{ km s}^{-1}$ . The spectra of this quasar are plotted in Fig. 1, where the red solid lines represent the pseudo-continua fittings. In Fig. 2, we show the pseudo-continuum normalized spectra. For this C IV absorption system, we expect to detect the absorptions caused by other metal species with relatively high abundances of ele-

**Table 1.** Measurements of C IV absorption systems

Species	$z_{\text{abs}}$	$W_r$ [Å]	$W_r^a$ [Å]
<i>C IV</i> $\lambda$ 1548	2.0053	$0.70 \pm 0.12$	0.13
<i>C IV</i> $\lambda$ 1551		$0.60 \pm 0.10$	0.11
<i>S I</i> $\lambda$ 1444		$0.29 \pm 0.05$	0.07
<i>Co II</i> $\lambda$ 1448		$0.42 \pm 0.07$	0.10
<i>N V</i> $\lambda$ 1238		$0.95 \pm 0.13$	...
<i>N V</i> $\lambda$ 1242		$1.51 \pm 0.19$	...
<i>Si II</i> $\lambda$ 1260		$1.24 \pm 0.08$	...
<i>Si II</i> $\lambda$ 1255		$1.11 \pm 0.17$	...
<i>S II</i> $\lambda$ 1253		$0.58 \pm 0.12$	...
<i>S II</i> $\lambda$ 1250		$0.36 \pm 0.09$	...
<i>C IV</i> $\lambda$ 1548	1.8011	$0.24 \pm 0.08$	0.08
<i>C IV</i> $\lambda$ 1551		$0.33 \pm 0.08$	0.08

<sup>a</sup>The equivalent width limits for the SDSS-I/II spectra.

ments. However, we find that there are only two appropriate lines (*S I*  $\lambda$ 1444 and *Co II*  $\lambda$ 1448), which have fallen into both the SDSS-I/II and SDSS-III spectra. However, many appropriate lines are located at the Ly $\alpha$  forest region and their wavelengths are not covered by the SDSS-I/II spectra. We invoke the Gaussian function to measure the equivalent widths at the rest frame of the detected absorption lines and we estimate their uncertainties using the Gaussian fittings. The fitting results are shown in Fig. 2 and presented in Table 1.

The question is whether the whole trough near to 1380 Å at the quasar rest frame, which was imprinted on the SDSS-III spectrum but not on that of the SDSS-I/II, was mainly caused by the absorption of the *Si IV*  $\lambda$ 1393, 1402 doublet. When the *Si IV*  $\lambda$ 1393, 1402 absorption doublet is located at the spectra region near to 1380 Å at quasar rest-frame, the wavelength separation of the *Si IV*  $\lambda$ 1393, 1402 doublet is  $\sim 9$  Å. However, the width of this whole absorption trough is only 7.3 Å at depths  $> 10\%$  below the continuum. Therefore, this trough is unlikely to be mainly caused by the absorption of the *Si IV*  $\lambda$ 1393, 1402 doublet. It can clearly be seen from Fig. 2 that the absorptions of *S I*  $\lambda$ 1444 and *Co II*  $\lambda$ 1448 alone, which are consistent with the R-component, cannot completely account for this trough. We invoke four Gaussian components to fit this trough, of which two account for the absorptions of *S I*  $\lambda$ 1444 and *Co II*  $\lambda$ 1448, which are consistent with the R-component. We find that the other two Gaussian components are consistent with the absorption of the *C IV*  $\lambda$ 1548, 1551 doublet located at  $z_{\text{abs}} = 1.8011$ . The fitting results are shown in Fig. 2 and presented in Table 1.

We also measure other obvious absorption lines, which are imprinted on both the SDSS-I/II and SDSS-III spectra of this quasar. These absorption lines can be divided into five intervening Mg II  $\lambda$ 2796, 2803 absorption systems. The fitting results are plotted in Fig. 2 and presented in Table 2.

**Table 2.** Measurements of Mg II absorption systems

Species	$z_{\text{abs}}$	$W_r^a$ [Å]	$W_r^b$ [Å]
<i>Mg II</i> $\lambda$ 2796	0.3635	$1.25 \pm 0.15$	$0.91 \pm 0.20$
<i>Mg II</i> $\lambda$ 2803		$1.18 \pm 0.15$	$0.81 \pm 0.25$
<i>Mg II</i> $\lambda$ 2796	0.4167	$0.82 \pm 0.13$	$0.48 \pm 0.13$
<i>Mg II</i> $\lambda$ 2803		$0.64 \pm 0.12$	$0.78 \pm 0.17$
<i>Mg II</i> $\lambda$ 2796	0.9634	$0.92 \pm 0.07$	$1.17 \pm 0.16$
<i>Mg II</i> $\lambda$ 2803		$0.82 \pm 0.08$	$0.77 \pm 0.10$
<i>Fe II</i> $\lambda$ 2600		$0.53 \pm 0.07$	$0.52 \pm 0.12$
<i>Fe II</i> $\lambda$ 2587		$0.16 \pm 0.05$	$0.24 \pm 0.10$
<i>Fe II</i> $\lambda$ 2383		$0.49 \pm 0.07$	$0.56 \pm 0.14$
<i>Fe II</i> $\lambda$ 2344		$0.25 \pm 0.06$	$0.25 \pm 0.12$
<i>Mn II</i> $\lambda$ 2004		$0.47 \pm 0.14$	$0.18 \pm 0.07$
<i>Mg II</i> $\lambda$ 2796	1.1484	$0.39 \pm 0.08$	$0.27 \pm 0.10$
<i>Mg II</i> $\lambda$ 2803		$0.23 \pm 0.05$	$0.19 \pm 0.06$
<i>Mg II</i> $\lambda$ 2796	1.3352	$0.69 \pm 0.06$	$0.78 \pm 0.10$
<i>Mg II</i> $\lambda$ 2803		$0.49 \pm 0.07$	$0.63 \pm 0.10$
<i>Al III</i> $\lambda$ 1854		$0.26 \pm 0.05$	$0.30 \pm 0.07$
<i>Al II</i> $\lambda$ 1670		$0.14 \pm 0.04$	$0.12 \pm 0.07$

<sup>a</sup>The measurements from the SDSS-III spectra.

<sup>b</sup>The measurements from the SDSS-I/II spectra.

### 3 DISCUSSIONS

#### 3.1 Coverage fraction

As we know from atomic physics, the optical depth ratio of the *C IV*  $\lambda$ 1548, 1551 doublet is  $\tau_{1548} : \tau_{1551} \approx 2 : 1$  (Savage & Sembach 1991; Verner et al. 1994). If the absorber completely occults the background emission sources, the optical depth ratio of the resonance doublet should be consistent with the value expected from the atomic physics. When the absorber partially occults the background line sources, the unocculted fluxes, perhaps together with the local emission of the absorber and the background photons scattered into our sightline, will result in a deviation of the optical depth ratio from the theoretical value (e.g., Wampler et al. 1995; Barlow & Sargent 1997; Hamann et al. 1997). In principle, the intrinsic absorber is often expected to partially cover the background emission sources, and the coverage fraction can be calculated from the residual intensities of the resonance doublet.

The effective coverage fraction ( $C_f$ ) accounts for the fraction of background photons that are obstructed by the absorbing gas at a given wavelength, and the effective optical depth ( $\tau$ ) of the absorbing gas is considered to be the photons that survive when the background photons pass through the absorbing gas. Considering the effective coverage fraction and the effective optical depth, the normalized residual intensity at a given wavelength is

$$R(\lambda) = [1 - C_f(\lambda)] + C_f(\lambda)e^{-\tau(\lambda)} \quad (1)$$

For the *C IV*  $\lambda$ 1548, 1551 doublet that has an optical depth ratio of 2 : 1, the effective coverage fraction can be expressed as

$$C_f(\lambda) = \frac{[R_r(\lambda) - 1]^2}{R_b(\lambda) - 2R_r(\lambda) + 1} \quad (2)$$

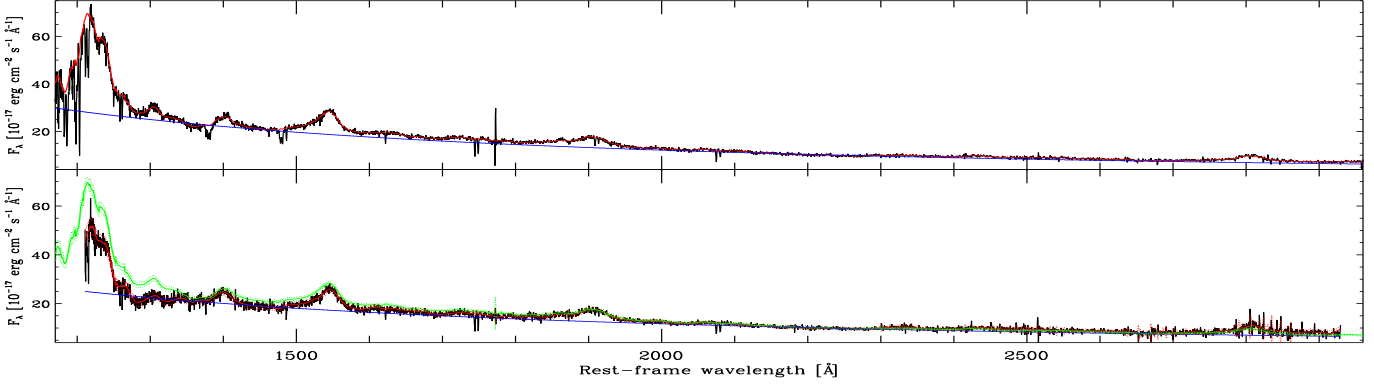


**Figure 1.** The spectra of quasar J095254.10+021932.8 with  $z_e = 2.1473$ . The blue solid lines represent the power-law continuum fittings. The lower panel is obtained by SDSS-I/II on 30 December 2000, and the upper panel is obtained by SDSS-III on 25 March 2011. The red solid lines represent the pseudo-continuum fittings, and the green solid line shown in the lower panel is just the pseudo-continuum plotted in the upper panel. The green/red dot-lines represent the corresponding pseudo-continuum fluxes accounting for the corresponding  $\pm 1\sigma$  flux uncertainties.

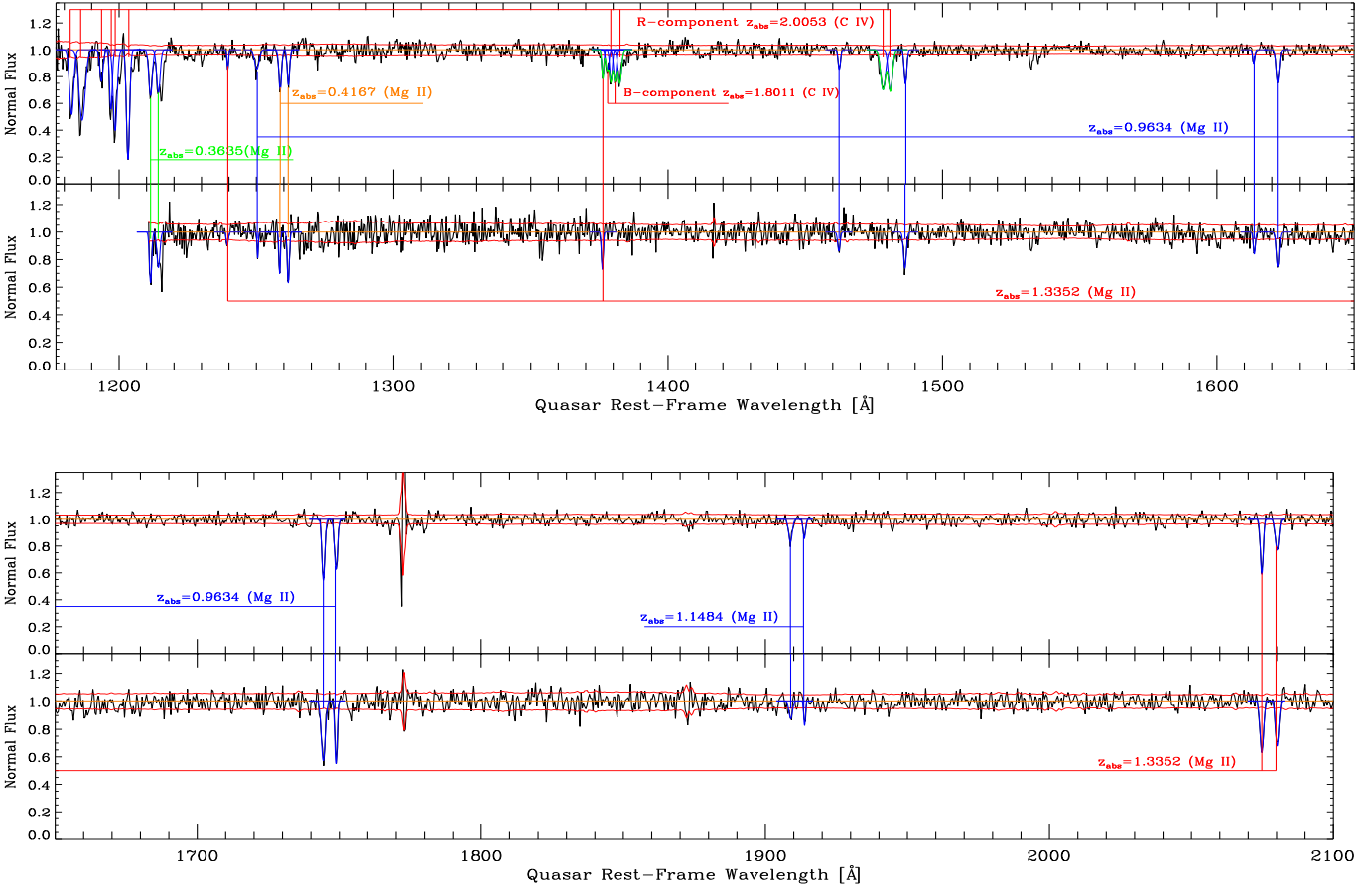


**Figure 2.** The pseudo-continua normalized spectra of quasar J095254.10+021932.8. The lower panel is obtained by SDSS-I/II, and the upper panel is obtained by SDSS-III. The red curves represent the flux uncertainty level which have been normalized by the corresponding pseudo-continua, the blue curves represent the Gaussian fittings. The green curves are just the sum of the multiple lines. The *R* – component is the C IV absorption system with  $z_{abs} = 2.0053$ , and The *B* – component is the C IV absorption system with  $z_{abs} = 1.8011$ . We also detect 5 *Mg II*  $\lambda\lambda 2796, 2803$  absorption systems with  $z_{abs} = 0.3635, 0.4167, 0.9634, 1.1484, \text{ and } 1.3352$ .

where the subscript  $r$  and  $b$  refer to the redder and bluer members of the C IV  $\lambda\lambda 1548, 1551$  doublet (see Hamann et al. 1997; Barlow & Sargent 1997; Ganguly et al. 1999; Misawa et al. 2007, for more detail).

It is well known that the emission from active galactic nuclei comes from multiple, separate components with different structures, such as the accretion disc, the broad emission-line region (BELR) and the narrow emission-line region (NELR). It is possible that the intrinsic absorber shows different coverage fractions for the different emission sources. For example, the absorber might partially cover the accretion disc but not cover the NELR, because the NELR is likely to be far away from the accretion disc. If we consider that the background photons, which pass through the absorber, are only from the continuum emission source and the BELR, and if we assume that the optical depths are the same from the two emission sources, the effective coverage fraction is the weighted average of the coverage fractions of the two emission sources, that is,

$$C_f = \frac{C_c + WC_e}{1 + W} \quad (3)$$

Here,  $C_c$  and  $C_e$  are the coverage fractions of the continuum emission source and the BELR, respectively, and  $W = f_e/f_c$  is the ratio of the broad-line flux-subtracted continuum flux to the continuum flux at the wavelength of the absorption line (e.g., Ganguly et al. 1999; Misawa et al. 2007; Wu et al. 2010). For background photons arising from more emission sources, see the discussions and the more general formalisms by Gabel et al. (2005) and Misawa et al. (2007). We can compute  $C_f$  of the C IV  $\lambda\lambda 1845, 1551$  absorber using the equation (2), and we can determine the value of  $W$  by measuring the strength of the broad emission line and the power-law continuum (which roughly depicts the emission from the accretion disc from UV to optical) at the position of the doublet. The values of  $C_c$  and  $C_e$  cannot be determined independently of each other, but we can derive a relation between them using the values of  $C_f$  and  $W$ .

For narrow absorption lines, it is inappropriate to compute the effective coverage fraction pixel by pixel using the low-resolution spectra of SDSS. Therefore, here we estimate the values of  $C_f$  of the  $R$ - and  $B$ -components using the normalized residual intensities at line cores. Thus, we obtain  $C_f = 0.30 \pm 0.05$  for the  $R$ -component and  $C_f = 0.17 \pm 0.04$  for the  $B$ -component.

The continuum emission from the accretion disc from UV to optical can be roughly described with a power-law function ( $f \propto \nu^{-\alpha}$ ). Adopting the method provided by Chen et al. (2009), we fit the power-law continuum by selecting several spectral regions without obvious emission lines, as shown in Fig. 1 by blue solid lines. We obtain  $\alpha = -1.68$  for the SDSS-III spectrum and  $\alpha = -1.51$  for the SDSS-I/II spectrum. It can be seen from the upper panel of Fig. 1 that the value of  $W$  would be less than 0.1 for both the  $R$ - and  $B$ -components. Adopting  $W = 0.1$ , together with the derived values of  $C_f$ , we can constrain the relations between the  $C_c$  and  $C_e$ , which are plotted in Fig. 3.

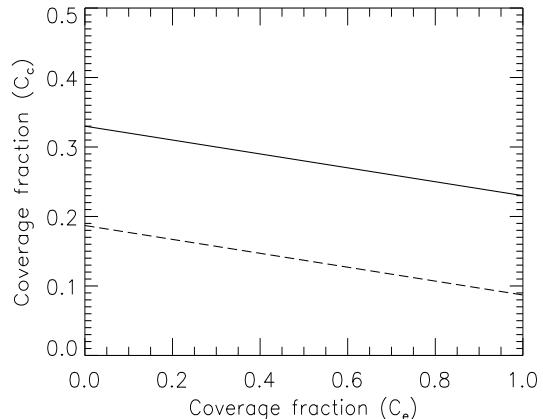


**Figure 3.** The  $C_c - C_e$  parameter plane. The solid line is for the  $R$ -component, and the dash line is for the  $B$ -component.

### 3.2 The properties of the emergence absorption systems

The time variation of the line strength and the partial coverage are the two most popular indicators to determine whether the absorber is truly intrinsic to the quasar. It can be clearly seen from Figs 1 and 2 that both the  $R$ -component and  $B$ -component show dramatic variations between the two SDSS observations. These dramatic variations, together with the effective coverage fractions that have been derived in Section 3.1, suggest that both the  $R$ -component and the  $B$ -component are likely to be intrinsic to the quasar.

The velocity offsets of the  $R$ -component ( $z_{\text{abs}} = 2.0053$ ) and the  $B$ -component ( $z_{\text{abs}} = 1.8011$ ), with respect to the quasar ( $z_e = 2.1473$ ), are  $\sim 13,800 \text{ km s}^{-1}$  and  $\sim 34,700 \text{ km s}^{-1}$ , respectively. Rough estimations from the curve of growth give rise to the column densities,  $N_{\text{H}}$ , would be greater than  $10^{17} \text{ cm}^{-2}$  for both the  $R$ - and  $B$ -components.

The quasar J095254.10+021932.8 was observed by SDSS-I/II on 2000 December 30, and by SDSS-III on 2011 March 25. The time interval of the two observations is 1186.4 d at the quasar rest frame. Because of the difference in focus of the BOSS quasars and standard stars, with respect to the SDSS-I/II spectra, the BOSS spectra usually exhibit excess flux at the bluer end and decrescent flux at the redder end (see fig. 5 of Pâris et al. 2012). This might explain the excess flux of the SDSS-III spectrum, with respect to the SDSS-I/II spectrum, at the blue end of the quasar J095254.10+021932.8 (see the red and green solid lines in the lower panel of Fig. 1). Taking into account this discrepancy, the quasar emissions (the pseudo-continua shown in Fig. 1) are stable for the two SDSS observations. We have derived the spectral indices of the power-law continuum for the SDSS-III and SDSS-I/II spectra,  $\alpha = -1.68$  and  $\alpha = -1.51$ , respectively. We believe that the discrepancy between the spectral indices can be mainly attributed to the excess flux at the bluer end and the decrescent flux at the redder end of the SDSS-III spectrum, rather than to the essence of the quasar. Therefore, the continuum emissions of the quasar J095254.10 +021932.8 should be very stable for the two SDSS observations. Together with the stable pseudo-

continua, the emissions of the broad lines (Si IV, C IV, C III and Mg II) should also be stable at the two epochs. In addition, when the bolometric luminosity ( $L_{\text{bol}}$ ) of the quasar is simply related to the monochromatic luminosity (e.g. the luminosity at  $\lambda 1350$ , Chen et al. 2011; Shen et al. 2012), the mass accretion rate would be also stable ( $\dot{M} \propto L_{\text{bol}}$ ).

Time variations of the intrinsic absorption lines seem to be common, but extreme events of the absorption-line emergence are very rare. We are aware that there have only been five previous reports that have observed the C IV absorption-line emergences via optical spectra (Ma 2002; Hamann et al. 2008; Leighly et al. 2009; Krongold et al. 2010; Rodríguez Hidalgo et al. 2011). All these studies have attributed the emergence events to the absorbers moving across the quasar sightlines. What are the origins of the R-component and B-component emerging from the spectrum of the quasar J095254.10+021932.8?

The question is whether the changes in the ionization state of the absorbing gas give rise to the emergence of absorption line. These changes can be caused by the following: (i) an increase in the incident flux, giving rise to photoionization from the lower ionization state to the higher ionization state (C III  $\rightarrow$  C IV); (ii) a decrease in the incident flux, causing recombination from the higher ionization state to the lower ionization state (C V  $\rightarrow$  C IV). The intrinsic absorption lines are often believed to originate in the outflow gas lifted off the accretion disc, and the C IV broad emission line region (Murray et al. 1995; Murray & Chiang 1997; Proga et al. 2000; Everett 2005). Here, we believe that the emergences of the C IV absorption doublets are unlikely to be a result of the ionization changes in the absorbing gas for the following reasons: (i) there is no evidence of remarkable changes in the observed power-law continuum; (ii) there is a lack of variation in the broad emission lines.

The new outflow, arising from the situation where there was previously no outflow at all, seems to be a reasonable explanation for the emergence of C IV absorption lines. Using equation (2) (i.e. reverberation mapping) of Kaspi et al. (2007), and together with the monochromatic luminosity at 1350 Å, we can estimate the radius of the C IV BELR as  $R_{\text{C IV}} \approx 0.33$  pc. Assuming that the C IV absorption lines form at a radii just beyond the C IV BELR, the characteristic flow times ( $t \sim R_{\text{C IV}}/v_r$ , where the  $v_r$  is the relative velocity of the absorber with respect to the quasar) would be  $t_1 \sim 23.7$  years for the *R* – component, and  $t_2 \sim 9.4$  years for the *B* – component. These flow times are much larger than the time interval of the two SDSS observations ( $\sim 3.3$  years). In addition, the stabilities of the power-law continuum emission and mass accretion rate might imply that there is no remarkable change in the structure of the accretion disc, which suggests that there is no new outflow. Therefore, the rise of a new outflow can be ruled out as an explanation for the extreme events surrounding the emergence of C IV absorption line.

The movement of the absorbing gas across the quasar sight-line probably accounts for the emergence of absorption troughs. The incomplete occultation of the background emission sources (see Section 3.1) implies that the sizes of the absorbers are small. Considering the case of a geometrically thin accretion disc and an optical thick accretion disc, most of the UV continuum radiation of the quasar is expected to arise from the inner accretion disc, whose size is

of the order of  $D_{\text{cont}} \sim 5R_S = 10GM_{\text{BH}}/c^2$  (Wise et al. 2004; Misawa et al. 2005; Chen et al. 2013). We directly adopt the virial black hole mass We directly adopt the virial black hole mass  $M_{\text{BH}} = 10^{9.56} M_{\odot}$ , which is estimated based on the C IV broad emission line (Shen et al. 2011), as the mass of the black hole. This results in  $D_{\text{cont}} = 5.35 \times 10^{15}$  cm. It can be seen from the  $C_c - C_e$  plane (Fig. 3) that the coverage fraction of the absorber to the continuum emission source is 23%  $\sim$  33% for the *R* – component, and 9%  $\sim$  19% for the *B* – component. Thus, we have a characteristic absorber radius of  $\sim 1.5 \times 10^{15}$  cm for the *R* – component, and  $\sim 0.7 \times 10^{15}$  cm for the *B* – component. Adopting the time interval of the two SDSS observations (i.e. 1186.4 d) as the upper limit of the transit time of the absorbing gas, we can estimate the lower limits of the transverse velocity perpendicular to the quasar sightline as  $\sim 146$  km s $^{-1}$  and  $\sim 73$  km s $^{-1}$  for the *R*– and *B* – components, respectively. Taking the virial black hole mass and assuming that the shift velocities of the absorbing gas do not exceed the escape velocities, we can derive the upper limits of the absorber distances relative to the central region: the absorber with  $z_{\text{abs}} = 2.0053$  locates at a radius of  $r \sim 0.82$  pc and the absorber with  $z_{\text{abs}} = 1.8011$  at a radius of  $r \sim 0.13$  pc. From our estimation, we know that the radius of the C IV BELR is  $R_{\text{C IV}} \sim 0.33$  pc. In this way, these absorbers would locate at the vicinity of the BELRE.

Radiation pressure, magnetohydrodynamic and thermal driving are all mechanisms that can be used to derive an outflow (Proga 2007). The question is what mechanism dominates the high-velocity outflow of the quasar J095254.10+021932.8. However, it is beyond the scope of this paper to accurately derive this mechanism. Ganguly et al. (2007) and Ganguly and Brotherton (2008) have found an up-per envelope curve for the relation between the maximum velocity of the outflow and the quasar luminosity (i.e.  $v_{\text{max}} \propto L^{0.662}$ ), which is expected from the radiation-driven outflow. We plot the  $v_{\text{max}} - L$  plane in Fig. 4 with the upper envelope curve. It is clear that the maximum velocity of the outflow of the quasar J095254.10+021932.8 is close to the upper envelope curve, which implies that the outflow might be dominated by radiation pressure.

Absorbers that are weakly ionized (e.g., C IV, N V, O VI) are often observed in X-ray and UV spectroscopic surveys, but no highly ionized absorbers (e.g., Mg VI, Fe XVII) have been detected in UV spectra. The absorption lines with low ionizations and low velocities, which are observed in both X-ray and UV spectra and have similar velocities, imply an underlying relation between the absorption lines in the UV spectra and those in the X-ray spectra (e.g., Mathur et al. 1994, 1995; Kaspi et al. 2002; Krongold et al. 2003; Gupta et al. 2013a). These absorption lines might be formed in a single outflow with multiple discrete components (e.g. Krongold et al. 2003, 2005, 2007). The component that is highly ionized gives rise to absorption lines at high energies, and the component that is weakly ionized produces X-ray and UV absorption lines. The narrow absorption-line outflows with ultra-high velocity and high ionization seem to be observed more often in X-ray spectra (e.g. Tombesi et al. 2010a,b, 2011a,b; Gupta et al. 2013b). These absorbers would be compact, located close to the black holes and would have values of column density as large as  $N_{\text{H}} = 10^{22} - 10^{24}$  cm $^{-2}$ . We note from fig. 6 of

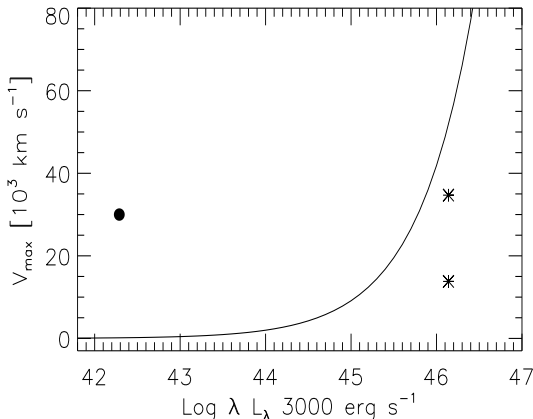


**Figure 4.** The maximum velocity of absorption vs the monochromatic luminosity at 3000 Å. The stars are for the data of this work, and the fill circle is for the data in Gupta et al. 2013b.

Gupta et al. (2013b) that most of these ultra-fast outflows lie well above the upper envelope curve. This suggests that the mechanism driving these ultra-fast outflows might differ from that of the out-flows that lie well below the upper envelope curve.

Recently, Gupta et al. (2013b) have become the first to detect an ultra-fast outflow in the soft X-ray spectra of Ark 564 using the O VI absorption line at the velocity of  $\sim 0.1c$ . This O VI absorption line has a similar velocity and ionization level as the C IV absorption lines that we have detected in this work. The value of the column density ( $N_{\text{H}}$ ) of this O VI absorber is  $10^{20} \text{ cm}^{-2}$ , which is much larger than the low limit value of the C IV absorbers ( $10^{17} \text{ cm}^{-2}$ ). Adopting the bolometric correction factor, one can roughly compute the monochromatic luminosity at 3000 Å from the bolometric luminosity of the Ark 564 (Shen et al. 2011), and plot the O VI ultra-fast outflow in the  $v_{\text{max}} - L$  plane (see the filled circle shown in Fig. 4). We can see from Fig. 4 that the O VI ultra-fast outflow lies well above the upper envelope curve, which is significantly different from the C IV outflow of this work. Therefore, the magnetohydrodynamic mechanism might dominate the O VI ultra fast outflow (Gupta et al. 2013b), unlike the radiation-pressure mechanism linked to the C IV outflow. Although some properties of the O VI ultra-fast outflow and the C IV outflow display obvious differences, the similar velocities and ionization levels might lead us to investigate the connection between the absorption lines in the UV spectra and those in the X-ray spectra. This precise connection would be complicated and is beyond the scope of this paper.

#### 4 CONCLUSIONS

The quasar J095254.10+021932.8 with  $z_e = 2.1473$  was observed by SDSS-I/II on 30 December 2000, and reobserved by SDSS-III on 25 March 2011. The time interval of the two observations is 1186.4 days at quasar rest-frame. We find that two C IV  $\lambda\lambda 1548, 1551$  narrow absorption systems, which are respectively located at  $z_{\text{abs}} = 2.0053$  (*R - component*) and  $z_{\text{abs}} = 1.8011$  (*B - component*), are

obviously imprinted on the SDSS-III spectrum. However, these two absorption systems can not be observed from the SDSS-I/II spectrum. With respect to the quasar, the velocities offset is  $\sim 13,800 \text{ km s}^{-1}$  for the *R - component*, and  $\sim 34,700 \text{ km s}^{-1}$  for the *B - component*. We also find that both the two absorbers partially occult the background emission sources. The effective coverage fraction is  $C_f = 0.30 \pm 0.05$  and  $C_f = 0.17 \pm 0.04$  for the *R - component* and *B - component*, respectively.

The stabilities of the continuum radiations and the broad emission lines of the quasar J095254.10+021932.8 suggest that the dramatic variations of absorption troughs are unlikely to be caused by the changes in the ionization state of the absorbing gas. In addition, considering the time interval of the two SDSS observations, a new outflow scenario, arising from the situation where there was previously no outflow at all, cannot account for the line variations of both the R-component and B-component.

The multiple streaming gas moving across our sightline might be the best explanation for the emergence of the two C IV absorption systems. Adopting the time interval of the two SDSS observations as the upper limit of the absorber transit time, we estimate the lower limits of the transverse velocity perpendicular to the line of sight. This gives rise to velocities of  $146 \text{ km s}^{-1}$  for the *R - component* and  $73 \text{ km s}^{-1}$  for the *B - component*. Assuming that the shift velocities of the absorbers do not exceed the escape velocities, the distances of the absorbers relative to the central region are  $\sim 0.82 \text{ pc}$  for the *R - component*, and  $\sim 0.13 \text{ pc}$  for the *B - component*. These absorbers might lie in the vicinity of the broad emission line region of the quasar ( $R_{\text{C IV}} \sim 0.33 \text{ pc}$ ).

We thank the anonymous referee for helpful comments and suggestions. This work was supported by the Guangxi Natural Science Foundation (2012jjAA10090), the National Natural Science Foundation of China (No. 11073007), and the Guangzhou technological project (No. 11C62010685).

#### REFERENCES

- Arav N., Li Z. Y., Begelman M. C., 1994, ApJ, 432, 62
- Abazajian K. N. et al., 2009, ApJS, 182, 543
- Barlow T. A., & Sargent W. L. W. 1997, AJ, 113, 136
- Bower R. G., Benson A. J., Malbon R., Helly J. C., Frenk C. S., Baugh C. M., Cole S., Lacey C. G., 2006, MNRAS, 370, 645
- Crenshaw D. M., Kraemer S. B., George I. M., 2003, ARA&A, 41, 117
- Chen Z. Y., Gu M. F.; Cao X. W., 2009, MNRAS, 397, 1713
- Chen Z. F., Chen Z. Y., Qin Y. P., Gu M. F., Lü L. Z., Su C. Y., Li Y. B., Chen Y., 2011, RAA, 4, 401
- Capellupo D. M., Hamann F., Shields J. C., Rodríguez Hidalgo P., Barlow T. A., 2011, MNRAS, 413, 908
- Capellupo D. M., Hamann F., Shields J. C., Rodríguez Hidalgo P., Barlow T. A., 2012, MNRAS, 422, 3249
- Capellupo D. M., Hamann F., Shields J. C., Halpern J. P., Barlow T. A., 2012, MNRAS, 422, 3249
- Chen Z. F., Qin Y. P., Gu M. F., 2013, ApJ, 770, 59

- Di Matteo T., Springel V., Hernquist L., 2005, *Nat*, 433, 604
- de Kool M. & Begelman M. C., 1995, *ApJ*, 455, 448
- Dunn Jay P., Arav Nahum, Aoki Kentaro, Wilkins Ashlee, Laughlin Courtney, Edmonds Doug, Bautista Manuel, 2012, *ApJ*, 750, 143
- Eisenstein D. J. et al., 2011, *AJ*, 142, 72
- Everett J. E., 2005, *ApJ*, 631, 689
- Filiz Ak N. et al., 2012, *ApJ*, 757, 114
- Ganguly R., Eracleous M., Charlton J. C., Churchill C. W., 1999, *AJ*, 117, 2594
- Gabel J., et al., 2005, *ApJ*, 623, 85
- Ganguly R., Scoggins B., Cales S., Brotherton M. S., Vestergaard M., 2007, *ApJ*, 665, 990
- Ganguly R. & Brotherton M. S., 2008, *ApJ*, 672, 102
- Gibson R. R., Brandt W. N., Schneider D. P., Gallagher S. C., 2008, *ApJ*, 675, 985
- Gupta A., Mathur S., Krongold Y., Nicastro F., 2013a, *ApJ*, 768, 141
- Gupta A., Mathur S., Krongold Y., Nicastro F., 2013b, *arXiv:1301.6139*
- Hamann F., Barlow T. A., Junkkarinen V., Burbidge E. M., 1997, *ApJ*, 478, 80
- Hamann F. & Sabra B., 2004, *ASPC*, 311, 203
- Hamann F., Kaplan K. F., Hidalgo P. R., Prochaska J. X., Herbert-Fort S., 2008, *MNRAS*, 391, L39
- Hamann F., Kanekar N., Prochaska J. K. et al., 2011, *MNRAS*, 410, 1957
- Jannuzi B. T. et al., 1996, *ApJ*, 470, L11
- Kaspi S., et al. 2002, *ApJ*, 574, 643
- King A., 2003, *ApJ*, 596, L27
- Krongold Y., Nicastro F., Brickhouse N. S., Elvis M., Liedahl D. A., Mathur S., 2003, *ApJ*, 597, 832
- Krongold Y., Nicastro F., Elvis M., Brickhouse N. S., Mathur S., Zezas A., 2005, *ApJ*, 620, 165
- Krongold Y., Nicastro F., Elvis M., Brickhouse N., Binette L., Mathur S., Jiménez-Bailón E., 2007, *ApJ*, 659, 1022
- Kaspi S., Brandt W. N., Maoz D., Netzer H., Schneider D. P., Shemmer O., 2007, *ApJ*, 659, 997
- Krongold Y., Binette L., Hernandez-Ibarra F., 2010, *ApJ*, 724, 203
- Laor A. & Brandt W. N., 2002, *ApJ*, 569, 641
- Lundgren B. F., Wilhite B. C., Brunner R. J. et al., 2007, *ApJ*, 656, 73
- Leighly K. M., Hamann F., Casebeer D. A., Grupe D., 2009, *ApJ*, 701, 176
- Murray N., Chiang J., Grossman S. A., Voit G. M., 1995, *ApJ*, 451, 498
- Mathur S., Wilkes B., Elvis M., Fiore F., 1994, *ApJ*, 434, 493
- Mathur S., Elvis M., Wilkes B., 1995, *ApJ*, 452, 230
- Murray N. & Chiang J., 1997, *ApJ*, 474, 91
- Ma F., 2002, *MNRAS*, 335, L99
- Moll R., Schindler S., Domainko W., Kapferer W., Mair M., van Kampen E., Kronberger T., Kimeswenger S., Ruffert M., 2007, *A&A*, 463, 513
- Misawa T., Eracleous M. D., Charlton J. C., Tajitsu A., 2005, *ApJ*, 629, 115
- Misawa T., Charlton J. C., Eracleous M., Ganguly R., Tytler D., Kirkman D., Suzuki N., Lubin D., 2007, *ApJS*, 171, 1
- Misawa T., Eracleous M., Chartas G., Charlton J. C., 2008, *ApJ*, 677, 863
- Moe M., Nahum Arav N., Bautista M. A., Korista K. T., 2012, *ApJ*, 706, 525
- Narayanan D., Hamann F., Barlow T., Burbidge E. M., Cohen R. D., Junkkarinen V., Lyons R., 2004, *ApJ*, 601, 715
- Nestor D. B., Turnshek D. A., Rao S. M., 2005, *ApJ*, 628, 637
- Nestor D., Hamann F., Rodriguez Hidalgo P., 2008, *MNRAS*, 386, 2055
- Proga D., Stone J. M., Kallman T. R., 2000, *ApJ*, 543, 686
- Proga D., 2007, *ASPC*, 363, 267
- Pâris I. et al., 2012, *A&A*, 548, 66
- Quider A. M., Nestor D. B., Turnshek D. A., Rao S. M., 2011, *AJ*, 141, 137
- Rodríguez Hidalgo P., Hamann F., Hall P., 2011, *MNRAS*, 411, 247
- Ross N. P. et al., 2012, *ApJS*, 199, 3
- Savage B. D. & Sembach K. R., 1991, *ApJ*, 379, 245
- Silk J. & Rees M. J., 1998, *A&A*, 331, L1
- Sabra B. M., Hamann F., Jannuzi B. T., George I. M., Shields J. C., 2003, *ApJ*, 590, 66
- Schneider D. P. et al., 2010, *AJ*, 139, 2360
- Shen Y., et al., 2011, *ApJS*, 194, 45
- Tombesi F. et al., 2010a, *ApJ*, 719, 700
- Tombesi F. et al., 2010b, *A&A*, 521, A57
- Tombesi F., Cappi M., Reeves J. M., Palumbo G. G. C., Braitto V., Dadina V., 2011a, *ApJ*, 742, 44
- Tombesi F., Sambruna R. M., Reeves J. M., Reynolds C. S., Braitto V., 2011b, *MNRAS*, 418, L89
- Verner D. A., Barthel D., Tytler D., 1994, *A&AS*, 108, 287
- Vivek M., Srianand R., Mahabal A., Kuriakose V.C., 2012, *MNRAS*, 421, L107
- Wampler E. J., Chugai N. N., Petitjean P., 1995, *ApJ*, 443, 586
- Weymann R. J., Morris S. L., Foltz C. B., Hewett P. C., 1991, *ApJ*, 373, 23
- William H. P., Teukolsky S. A., William T. V., Flannery B. P., 1992, *Numerical Recipes in Fortran: The Art of Scientific Computing*. Cambridge Univ. Press, p107
- Wise J. H., Eracleous M., Charlton J. C., Ganguly R., 2004, *ApJ*, 613, 129
- Wu J., Charlton J. C., Misawa T., Eracleous M., Ganguly R., 2010, *ApJ*, 722, 997
- York D. G. et al., 2000, *AJ*, 120, 1579
- Yuan Q., Green R. F., Brotherton M., Tripp T. M., Kaiser M. E., Kriss G. A., 2002, *ApJ*, 575, 687